IEEE Access
Multidisciplinary | Rapid Review | Open Access Journal

Received July 1, 2020, accepted August 10, 2020, date of publication August 14, 2020, date of current version August 26, 2020.

Digital Object Identifier 10.1109/ACCESS.2020.3016646

Design of a Rotary-Linear Motor With Unipolar SPM and Voice Coil Structure

FUZHEN XING, (Student Member, IEEE), AND BYUNG-IL KWON, (Member, IEEE)
Energy Conversion Systems Laboratory, Hanyang University, Ansan 15588, South Korea

Corresponding author: Byung-Il Kwon (bikwon@hanyang.ac.kr)

This work was supported in part by the Ministry of Trade, Industry and Energy, South Korea, through the Human Resources Program in Energy Technology of the Korea Institute of Energy Technology Evaluation and Planning (KETEP), under Grant 20154030200730; and in part by the National Research Foundation of Korea through the BK21PLUS Program within the Ministry of Education.

ABSTRACT In this article, a rotary-linear motor that achieves rotary and linear motions with a simple one-air-gap structure, low rotary ripple, and smooth linear force is proposed. The proposed motor combines a five-phase unipolar surface-mounted permanent-magnet (USPM) and a voice coil structure to simplify the motor structure, which motor can be named as rotary-linear surface-mounted permanent-magnet voice coil motor (RL-SVCM). And because of the characteristics of the rotary five-phase armature circuit and linear voice coil circuit, the proposed motor can provide low rotary ripple and smooth linear force. For designing the motor, the magnetic equivalent circuit (MEC) method is used to study the relationship between the linear force performance and motor structure parameters, and the effect of the flux bridges on the linear force and rotary torque. Due to uncertain variables in MEC, the FEM method is used to analyze the precise output result of rotary torque and linear force, and non-interaction between rotary and linear motions.

INDEX TERMS Rotary-linear motor, two-degree-of-freedom motion, voice coil motor (VCM).

I. INTRODUCTION

A conventional electrical motor can only work in a rotary or a linear motion as a single-degree-of-freedom motor. Therefore, in some applications that require both rotary and linear motion, the conventional approach just makes the single-degree-of-freedom motor shaft mechanically connected axially for a multiple-degrees-of-freedom motion [1]–[3]. However, this can no longer satisfy the customer requirements for a low torque ripple, a smooth linear force, non-interaction control strategy, and a simple motor structure with a small machine size. Just like the motor works in small high-precision robot arms and chip assembly systems.

A rotary-linear motor can mainly be divided into two types based on the magnetic flux circuit field structure, namely, a crossed rotary-linear (RL) magnetic field and an independent RL magnetic field. A classical two-degree-of-freedom (2DoF) motor with a crossed-coupled magnetic field was proposed in [4]. This motor structure makes the most of the magnetic core space, and it has a high output torque and force. However, its armature coil is quite complicated, and the rotor/mover structure is very wasteful of PMs. In [5], a 2DoF motor with a single stator is proposed. However, there is a large magnetic field coupling reaction between the rotary motion and linear motion. Moreover, because a doubly salient topology is utilized, huge rotary torque ripple and linear force ripple are also issues that need to be overcome. Another 2DoF RL motor [6], [7] is composed of two arc-shaped stators of the rotary and linear parts, respectively, and a solid rotor coated with a copper layer. Moreover, the proposed 2DoF split-stator induction motor with a solid mover is easy to manufacture at low cost, although the efficiency should be improved further for an industrial application. In addition, in a double-stator RL PM motor [8]–[10], the coupling effect is generated at the ending parts with a double-layer air gap. With this motor, the coupling effect varies with the excitation currents in the orthogonal crossed magnetic field. By setting suitable values for the orthogonal fluxes, the coupling effect can be reduced.

Another type of multi-stator 2DoF RL motor with independent RL magnetic fields is shown in [11], which is comprised of a three-phase 6/4 rotary SRM and a two-phase transverse flux linear SRM. Fixed translators are adopted to reduce the mechanical coupling effect by avoiding the negative torque produced by the magnetic field induced in the translator. Apart from this, the main way to decouple the rotary and

The associate editor coordinating the review of this manuscript and approving it for publication was Zhuang Xu.

linear modules is realized through decoupled control. However, this creates a waste of space on complex structures. A novel 2DoF voice coil motor with independent magnetic fields has thus been proposed [12], [13]. An armature is composed of two windings corresponding to the linear and rotary motions, respectively. It was concluded that the motor has two independent magnetic fields for two motions. However, its structure is slightly complicated, and its movement is dependent on the mechanical structure. The aforementioned RL-motors exhibit the common disadvantages of an incomplete complex control, a large weight and size, and a high force and torque ripple.

In this study, a rotary-linear SPM voice coil motor (RL-SVCM) combined with a USPM and a voice coil [14]–[16] structure is proposed, which aims to achieve a low torque ripple, a smooth linear force, a simple structure, and no interaction between the linear and rotary motions. The structure of the motor under an easy design strategy is interpreted. For designing the motor, the magnetic equivalent circuit (MEC) method is used to analyze the relationship between the linear force performance and motor structure parameters, and also study the effect of the flux bridges on the linear force and rotary torque. Due to uncertain variables from the flux bridge in MEC, the FEM method is used to get the precise output result of rotary torque and linear force. The FEM result displays the low torque ripple, smooth linear force, and non-interaction between rotary and linear motions.

II. TOPOLOGY AND OPERATION PRINCIPLE

A. TOPOLOGY OF RL-SVCM

A unipolar surface-mounted permanent-magnet (USPM) motor and a voice coil motor have the same PM mounting strategy (PM mounted on the surface of the rotor). Thus, the USPM motor structure was selected in a rotary motion to collaborate with the voice coil motor structure during linear motion. The same magnet arrangement strategy provides significant cooperation in simplifying the motor structure, increasing the utilization rate of the material, and decreasing the RL-SVCM volume.

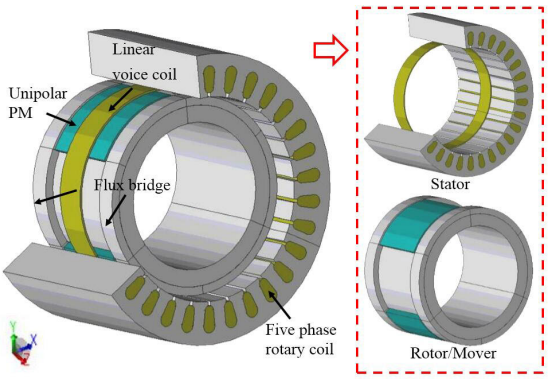

FIGURE 1. Proposed RL-SV CM structure in 3D.

As shown in figure 1, the proposed RL-SVCM model has only one air-gap structure, and the rotor/mover is equipped with three pieces of unipolar flux PM (in green). In addition, these unipolar PMs operate for both rotary and linear motions. The outside stator is equipped with two control circuits. One is the five-phase windings [17]–[19] inserted in the stator slot, and the other is the voice coil circuit stuck onto the inside face of the stator.

In particular, two sets of flux bridges are designed at each end of the rotor/mover for the linear motion, which can apply a linear motion magnet flux from the mover to the stator. In other words, the flux bridges and voice coil are equipped in the USPM motor, allowing the USPM motor to achieve linear motion. This strategy greatly simplifies the rotary linear motor structure. However, the addition of the flux bridges will cause a leakage flux, which will have an effect on the linear and rotary operations. These effects are discussed herein.

Above all, the RL-SVCM is based on one air-gap, one rotor/mover, and one stator structure. This design strategy not only achieves a full utilization of the magnet but also simplifies the motor structure and reduces the machine size.

B. OPERATING PRINCIPLE

The voice coil motor in a linear motion follows the principle of ampere force. When the current flows in the coil under a unipolar magnetic field, the coil suffers a force proportional to the in-flow current, as $F = kBILN$, where k is a constant, B is the field strength, I is the in-flow current, and L and N are the length and number of the conductor in the magnetic field, respectively. Hence, the voice coil structure is designed based on the operating principle of this voice coil motor in the proposed RL-SVCM, as shown in 2D in figure 2(a). Therefore, the stator, voice coil winding on the inside of the stator, rotor/mover with a unipolar PM, and two sets of flux bridges assist in the linear motion of the RL-SVCM.

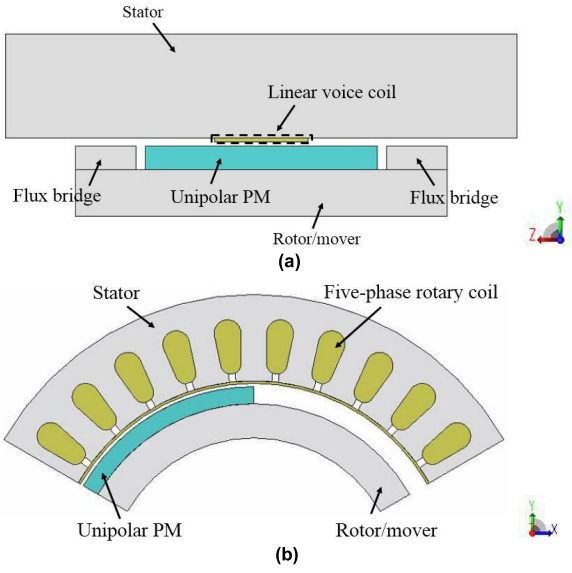

FIGURE 2. Proposed RL-SVCM structure in 2D: parts of RL-SVCM involved in (a) linear and (b) rotary motions.

A stator with five-phase distributed windings and a rotor/mover with a unipolar PM assist in the rotary motion

of the RL-SVCM, as shown in 2D figure 2(b). Because the voice coil winding and two sets of flux bridges are not involved in the rotary motion, they are not shown to facilitate a better understanding. These components in figure 2(b) form a unipolar SPM motor. In addition, the five-phase distributed winding in the stator is utilized for a low torque ripple during the rotary motion.

The axial rotary five-phase current (along the z-axis) and the tangential linear voice coil current (along the x-axis) in the stator are maintained in an orthogonal array. Therefore, when these two currents are simultaneously subjected to a radial magnet flux (along the y-axis), the rotor/mover can generate tangential rotary torque (along the x-axis) and an axial linear force (along the z-axis). They also maintain the orthogonal structure. Moreover, the rotary current is a sinusoidal current, whereas the linear voice coil current is a constant direct current. The linear motion constant direct current magnetic field will not affect the rotary motion five-phase current magnetic field. Therefore, the rotating magnetic field and the linear magnetic field do not theoretically affect each other.

III. MEC ANALYSIS OF RL-SVCM

A. MEC ANALYSIS OF LINEAR MOTION

To explore the detailed relationship between the performance of the linear motion force and the RL-SVCM structure parameters, the MEC method is used for analysis.

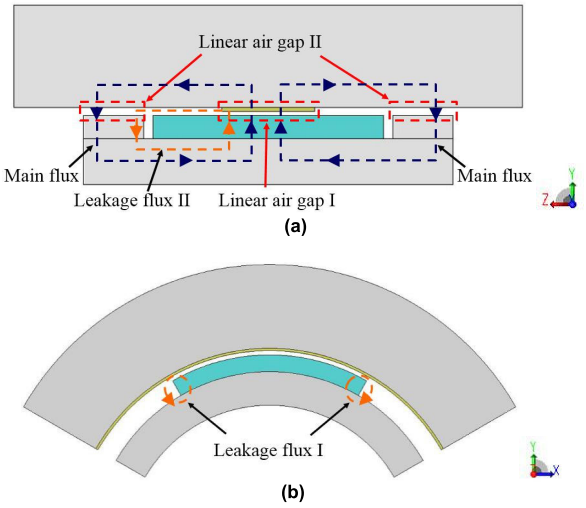

FIGURE 3. RL-SVCM linear motion flux line distribution at midpoint; (a) the main flux; (b) the leakage flux I.

1) DERIVATION OF LINEAR FORCE FORMULA

The linear motion working principle follows a voice coil motor model. In addition, the linear motion magnetic flux circuit is shown in figure 3. Figure 3(a) shows the main flux line distribution, and figure 3(b) shows a leakage flux I distribution. The equivalent magnetic circuit is illustrated in figure 4,

where Λ_σ is the permeance of leakage flux I and II, ϕ_σ is the leakage magnetic flux I and II, ϕ_δ is the magnetic flux in an air gap, Λ_{L1} and Λ_{L2} are the left part of the stator and rotor axial steel sheet permeance, Λ_{R1} and Λ_{R2} are the right part of the stator and rotor axial steel sheet permeance, $\Lambda\delta_1$ and $\Lambda\delta_2$ are the permeance of air-gap I and air-gap II, respectively.

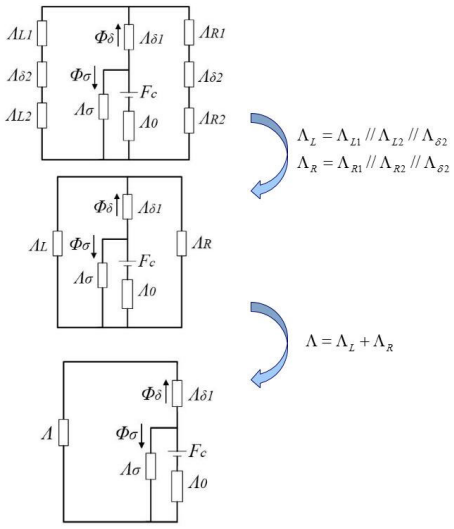

FIGURE 4. Simplified equivalent magnetic circuit flow.

When the motor is operated under linear motion, the rectangular magnetic circuit structure remains unchanged. Hence, for easy calculation, Equation (1) is used:

$$\begin{cases} \Lambda_L = \Lambda_{L1} // \Lambda_{L2} // \Lambda_{\delta 2} \\ \Lambda_R = \Lambda_{R1} // \Lambda_{R2} // \Lambda_{\delta 2} \end{cases} \tag{1}$$

In addition, structural permeance Λ can be defined as follows:

$$\Lambda = \Lambda_L + \Lambda_R \tag{2}$$

Hence, when combining Equations (1) and (2), figure 4 shows a simplified equivalent magnetic circuit flow.

In addition, according to the MEC in figure 4, the following is obtained:

$$\begin{cases} F_c \Lambda_0 = \varphi_\delta + \varphi_\sigma \\ \dfrac{\varphi_\delta}{\Lambda_{\delta 1} // \Lambda} = \dfrac{\varphi_\sigma}{\Lambda_\sigma} \end{cases} \tag{3}$$

where F_c is the magnet motive force of the permanent magnet, and Λ_0 is the permeance of the permanent magnet.

The magnetic flux in the air gap can be given as follows:

$$\phi_\delta = \frac{F_c \Lambda_0}{1 + \Lambda_\sigma (1/\Lambda + 1/\Lambda_{\delta 1})} \tag{4}$$

In addition,

$$\begin{cases} \Lambda_0 = \mu_r \mu_0 A_m / h_m \\ \Lambda_{\delta 1} = \mu_0 A_{\delta 1} / \delta_1 \\ F_c = H_c h_m \\ \varphi_\delta = B_\delta A_m \\ F_l = N_L B_\delta I_L L_r \end{cases} \tag{5}$$

where $\mu 0$ is the permeability of a vacuum, μ_r is the relative magnetic permeability of the permanent magnets, A_m is the cross-sectional area of the magnetic flux excited by the permanent magnets, h_m is the magnetization length of the permanent magnet in the linear section, $A_{\delta 1}$ is the cross-sectional area of the air gap, δ_l is the length of the mechanical

air gaps in the linear section, H_c is the coercive force of the permanent magnet, B_δ is the magnetic flux density in the linear section air gap I, N_L is the number of turns in the voice coil, I_L is the current in the conductors, and L_r is the average circumference of the coil.

Hence, the Lorenz force is calculated as follows:

$$F_l = \frac{\varphi_\delta N_L I_L L_r}{A_m} = \frac{H_c \mu_r \mu_0 N_L I_L L_r}{1 + (\Lambda_o + \Lambda_\sigma)(\frac{1}{\Lambda} + \frac{1}{\Lambda_{\delta 1}})} \tag{6}$$

From (5) and (6), because $\Lambda_{\delta 1}$ and the other parameters are constant, the linear Lorenz force F_l will only be influenced by the equivalent structure permeance Λ, and the leakage flux permeance Λ_σ.

2) ANALYSIS OF EQUIVALENT STRUCTURE PERMEANCE Λ

From Equations (1) and (2), the equivalent structure permeance Λ consists of axial steel sheet permeances $\Lambda L1$, Λ_{L2}, Λ_{R1}, and Λ_{R2} and air-gap II permeance $\Lambda_{\delta 2}$. Because a silicon steel sheet is axially laminated, the values of Λ_{L1}, Λ_{L2}, Λ_{R1}, and Λ_{R2} are relatively small and cannot be ignored.

In addition, based on figure 4, Λ_C is defined as follows:

$$\begin{cases} \Lambda_C = \Lambda_L // \Lambda_R \\ \frac{1}{\Lambda_C} = \frac{2}{\Lambda_{\delta 2}} + \Lambda_{L1} + \Lambda_{L2} + \Lambda_{R1} + \Lambda_{R2} = \frac{2}{\Lambda_{\delta 2}} + kL_S \end{cases} \tag{7}$$

where $1/\Lambda_C$ is the sum of $1/\Lambda_L$ and $1/\Lambda_R$, k is the permeance factor, and L_S is the axial length of the mover. Thus, Λ_c is not affected by the axial position of the linear motion. Combining Equations (2) and (7), a parabolic function between Λ and Λ_L is shown in figure 5, the equation of which is as follows:

$$\frac{1}{\Lambda} = f(\frac{1}{\Lambda_L}) = -\Lambda_c(\frac{1}{\Lambda_L})^2 + \frac{1}{\Lambda_L} \tag{8}$$

where Λ_L will change when the motor runs to different axial positions. Therefore, because $1/\Lambda_L = 1/\Lambda_R = 1/(2\Lambda_C)$, $1/\Lambda$ will reach the maximum value. To simplify the calculations, the following is defined:

$$\frac{1}{\Lambda_L} = \frac{1}{2\Lambda_C} + kx \tag{9}$$

where x is the distance between the axial midpoints of the mover and stator (as $x \leq Ls/2$). Thus, (9) can be used to represent the sum of $1/\Lambda_{L1}$ and $1/\Lambda_{L2}$ at different axial positions. The symmetry axis of the parabola coincides with the $1/\Lambda$-axis in figure 6. Hence,

$$\begin{aligned} \frac{1}{\Lambda} &= f(x) = -\Lambda_c(kx)^2 + \frac{1}{4\Lambda_C} \\ &= -\frac{\Lambda_{\delta 2}(kx)^2}{2 + kL_S\Lambda_{\delta 2}} + \frac{kL_S}{4} + \frac{1}{2\Lambda_{\delta 2}} \end{aligned} \tag{10}$$

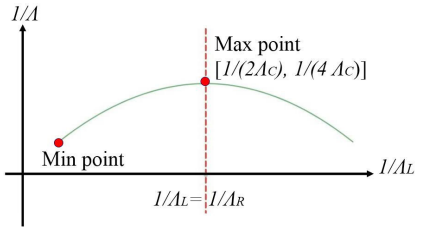

FIGURE 5. Parabolic relationship between 1/Λ and 1/ΛL.

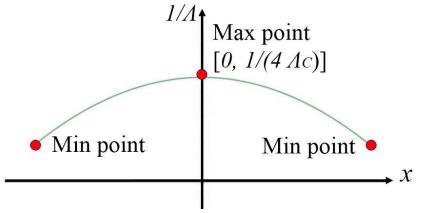

FIGURE 6. Parabolic relationship between 1/Λ and x.

The maximum value within a symmetry interval is as follows:

$$(\frac{1}{\Lambda})\max = f(\frac{1}{2\Lambda_C}) = \frac{1}{4\Lambda_C} = \frac{1}{2\Lambda_{\delta 2}} + \frac{kL_S}{4} \tag{11}$$

The minimum value within a symmetry interval is the following:

$$(\frac{1}{\Lambda})\min = f(\frac{1}{2\Lambda_C} - \frac{kL_S}{2}) \tag{12}$$

Therefore, the average value within a symmetry interval is as follows:

$$\begin{aligned} (\frac{1}{\Lambda})\text{average} &= \frac{1}{kL_S/2}\int_{\frac{1}{2\Lambda_C} - kL_S/2}^{\frac{1}{2\Lambda_C}} f(\frac{1}{\Lambda_L})d(\frac{1}{\Lambda_L}) \\ &= \frac{3(\frac{2}{\Lambda_{\delta 2}} + kL_S)^2 - (kL_S)^2}{12(\frac{2}{\Lambda_{\delta 2}} + kL_S)} \end{aligned} \tag{13}$$

In addition, the ripple within a symmetry interval is the following:

$$\begin{aligned} (\frac{1}{\Lambda})ripple &= \frac{(\frac{1}{\Lambda})\max - (\frac{1}{\Lambda})\min}{(\frac{1}{\Lambda})\text{average}} \\ &= \frac{(kL_S)^2}{\left(\frac{3-\sqrt{3}}{2\Lambda_{\delta 2}} + kL_S\right) * \left(\frac{3+\sqrt{3}}{2\Lambda_{\delta 2}} + kL_S\right)} \end{aligned} \tag{14}$$

Observations (13) and (14) show that the average value and ripple of $1/\Lambda$ are both functions of $\Lambda_{\delta 2}$ and L_S. In addition, if $\Lambda_{\delta 2}$ stays the same, the following relationships occur:

$$\begin{cases} L_S \searrow, & \Lambda_{average} \nearrow \\ L_S \searrow, & \Lambda_{ripple} \searrow \end{cases} \tag{15}$$

3) ANALYSIS OF LEAKAGE FLUX PERMEANCE $\Lambda\Sigma$

The magnitude of the permeance Λ_σ will be affected by the axial position.

When the voice coil is not near the flux bridge, as shown in figure 3, Λ_σ is mainly due to the flux leakage I. Flux leakage II is extremely small. In addition, Λ_σ can be ignored.

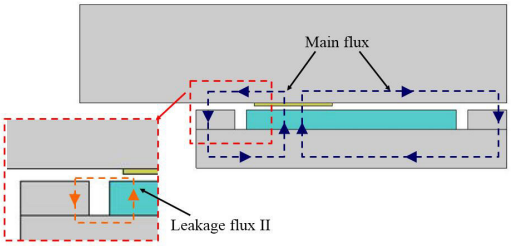

FIGURE 7. RL-SVCM linear motion flux line distribution at endpoint.

When the voice coil is near the flux bridge, as shown in figure 7, Λ_σ is not only from flux leakage I, but also from flux leakage II. Hence, Λ_σ increases with a decreasing distance between the voice coil and flux bridge. In addition, the change in Λ_σ cannot be accurately estimated.

4) LINEAR FORCE EFFECT BY Λ AND $\Lambda\Sigma$

When the voice coil is not near the flux bridge, Λ_σ remains the same. The linear force only changes with Λ. Combining Equation (6), the following is obtained:

$$\Lambda \propto F_l \tag{16}$$

In addition, the linear force can be rewritten as

$$\begin{aligned} F_l &= \frac{\varphi_\delta N_L I_L L_r}{A_m} \\ &= \frac{H_c \mu_r \mu_0 N_L I_L L_r}{1+(\Lambda_o+\Lambda_\sigma)(-\frac{\Lambda_{\delta 2}(kx)^2}{2+kL_S\Lambda_{\delta 2}}+\frac{kL_S}{4}+\frac{1}{2\Lambda_{\delta 2}}+\frac{1}{\Lambda_{\delta 1}})} \end{aligned} \tag{17}$$

From Equation (15), the following is obtained:

$$\begin{cases} L_S \searrow, & \Lambda_{\min} \propto F_{\min} \nearrow \\ L_S \searrow, & \Lambda_{average} \propto F_{average} \nearrow \\ L_S \searrow, & \Lambda_{ripple} \propto F_{ripple} \searrow \end{cases} \tag{18}$$

Hence, the linear force is proportional to the permeance Λ. The force axial distribution will form an arc with an upward opening, and reach a minimum point at the axial midpoint. From a design perspective, smaller motor axial lengths Ls will lead to a greater linear output force and a smaller force ripple.

When the voice coil is near the flux bridge, Λ_σ increases with a decreasing distance between the voice coil and flux bridge. However, Λ continues increasing during this interval. It is therefore difficult to analyze the change in linear force using the MEC under this situation.

B. MEC ANALYSIS OF ROTARY MOTION

The working principle of the rotary motion is mainly based on a traditional SPM motor, which has been analyzed in detail using MEC in numerous studies [20]–[23]. Differing from an RL-SVCM, there are two sets of flux bridges at the axial ends of the rotor, which is close to the PM and will generate a flux leakage, as compared with a traditional SPM motor. Thus, the effect of the flux leakage in a rotary motion is analyzed using MEC in this section.

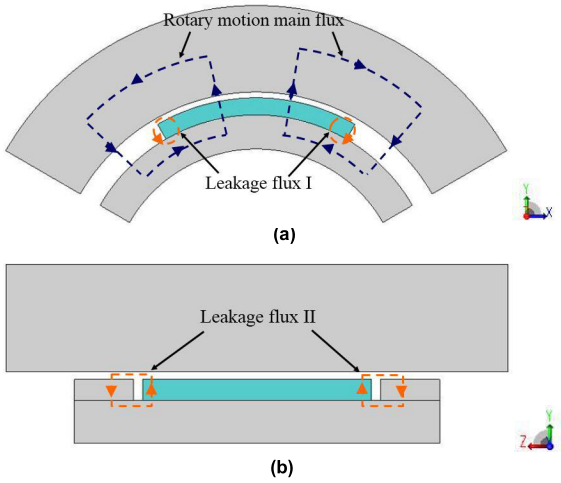

FIGURE 8. Rotary motion flux line distribution; (a) the main flux and leakage flux I on the radial section; (b) the leakage flux II on the axial section.

An RL-SVCM will create two magnetic flux circuits in two directions. One is the main rotary motion flux line distribution and leakage flux I in the radial section, as shown in figure 8(a). Here, the main flux is used to generate a rotary magnetic field and participate in creating a rotary torque. The other circuit is leakage flux II among the PM and flux bridges in the axial section, as shown in figure 8(b), which weakens the magnetic field potential of the PM. According to figure 8, a MEC diagram combining the radial main flux and the axial leakage flux is as shown in figure 9.

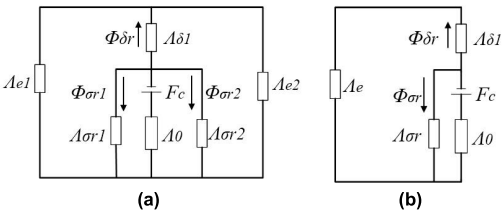

FIGURE 9. Equivalent magnetic circuit of rotary motion; (a) the original equivalent magnetic circuit; (b) the simplified equivalent magnetic circuit.

In addition, consider the following:

$$\begin{cases} \Lambda_e = \Lambda_{e1} // \Lambda_{e2} \\ \Lambda_{\sigma r} = \Lambda_{\sigma r1} // \Lambda_{\sigma r2} \end{cases} \tag{19}$$

where $\Lambda_{\sigma r}$ is the permeance of the rotary motion leakage magnetic flux, and Λ_e is the permeance of the air gap in a vacant magnet position. From (19), the equivalent circuit in

figure 9(a) can be changed to that shown in figure 9(b).

$$\begin{cases} F_c\Lambda_0 = \varphi_{\delta r} + \varphi_{\sigma r} \\ \dfrac{\varphi_{\delta r}}{\Lambda_{\delta r}//\Lambda_e} = \dfrac{\varphi_{\sigma r}}{\Lambda_{\sigma r}} \end{cases} \tag{20}$$

where $\phi_{\delta r}$ is the magnetic flux in the air gap, and $\phi_{\sigma r}$ is the leakage flux of the ending part flux bridge.

It can be inferred that the existence of leakage flux $\phi_{\sigma r}$ reduces the amount of main flux that passes through the air gap, which decreases the torque compared with an SPM motor without flux bridge.

IV. RL-SVCM DESIGN AND FEM ANALYSIS

A. DESIGN OF A RL-SVCM

Based on MEC analysis result of equation (17) and the conventional rotary motor D^2L design method [24]–[26]:

$$\begin{cases} \dfrac{D^2 l_{ef} n}{p'} = \dfrac{D^2 l_{ef} n}{T' \frac{2\pi n}{60}} = \dfrac{60/\pi^2}{\alpha_p K_{Nm} K_{\delta p} A B_\delta} \\ \mathrm{A} = \dfrac{2mN_R I_R}{\pi D} \end{cases} \tag{21}$$

After referring to [27]–[29], due to the simple structure of the motor, consider the size of some parameters like the thickness of the flux bridge at the end of the motor, the air gap next to the flux bridge, and the thickness of the rotor core. An RL-SVCM was designed, the detailed parameters of which are shown in Table 1.

TABLE 1. Electric machine parameters of RL-SVCM.

Item	Unit	Value
Stator slots	-	30
Magnet poles	-	3
Stator axial length	mm	110
Rotor axial length	mm	80
Stator in/outside diameter	mm	119.4/170
Voice coil in/outside diameter	mm	117.4/119.4
Rotor/mover in/outside diameter	mm	96/116
Linear motion active moving length	mm	30
PM length	mm	50
Flux bridge width (each)	mm	13
Air gap (between PM and flux bridge)	mm	2
Rotary coil turns (each slot)	n	250
Voice coil turns	n	20
Air gap length	mm	0.7
Rate rotary speed	n/min	1800
Rate linear speed	m/s	0.006

Here, m is the phase number of the rotary armature winding, α_p is the pole-arc coefficient, K_{Nm} is the wave shape coefficient of the air-gap magnetic field, $K_{\delta p}$ is the armature winding coefficient, D is the diameter, l_{ef} is the effective axial length of the armature winding, and I_R is the five-phase current of the rotary armature.

However, because Λ_σ is affected by the distance between the voice coil circuit and the flux bridges, and the value of Λ_σ cannot be estimated, the impact of the change in Λ_σ is ignored in the analysis results of the MEC linear force. In other words, the effect of magnetic leakage flux II is ignored in the results. Therefore, the FEM method when considering changes to all parameters is used for a precision analysis.

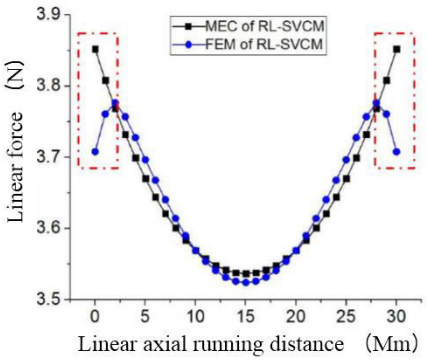

FIGURE 10. Comparison of linear force distribution of FEM and MEC.

B. FEM ANALYSIS OF LINEAR FORCE

The simulation results of the linear force distribution are shown in figure 10. The MEC results are based on Equation (17) without considering a change in Λ_σ, and the FEM result is based on a 3D RL-SVCM model considering such a change.

1) VOICE COIL NOT NEAR THE FLUX BRIDGE

In the axial interval of 2–28 mm, where the voice coil is not near the flux bridge, Λ_σ is only influenced by the leakage flux I. The shape of the two force curves is an arc with an upward opening, reaching the minimum at the axial midpoint. From Table 2, the average forces (2–28 mm) of the MEC and FEM are 3.617 and 3.626 N, which is an error of only 0.2%. In addition, the force ripple (2–28 mm) is 6.4% and 6.9%, respectively. After comparison, the two curves are found to be completely coincident.

TABLE 2. Electric machine parameter of RL-SVCM.

Item	Unit	FEM	MEC
Max linear force (2–28 mm)	N	3.776	3.768
Min linear force (2–28 mm)	N	3.524	3.536
Max linear force (0–30 mm)	N	3.776	3.852
Min linear force (0–30 mm)	N	3.524	3.536
Average linear force (2–28 mm)	N	3.626	3.617
Linear force ripple (2–28 mm)		6.9%	6.4%
Average linear force (0–30 mm)	N	3.640	3.645
Linear force ripple (0–30 mm)		6.9%	8.7%

2) VOICE COIL NEAR THE FLUX BRIDGE

In the axial intervals 0–2 mm and 28–30 mm, where the voice coil is near the flux bridge, Λ_σ increases gradually.

In addition, from figure 10, the MEC result is calculated without considering the leakage flux II from the flux bridges. Thus, the linear force of the MEC result continues to increase in the axial intervals of 0–2 mm and 28–30 mm. However, in the FEM result, the linear force decreases gradually owing to the influence of the magnetic leakage flux II. In Table 2, the average forces (0–30 mm) of the MEC and FEM are 3.645 and 3.640 N, which is an error of 0.14%. In addition, the force ripple (0–30 mm) is 8.7% and 6.9%, respectively. Both of the force analysis results show a smooth force ripple. Although the leakage flux II from the bridges slightly reduces the average force, it also reduces the force ripple in a relative manner.

C. FEM ANALYSIS OF ROTARY TORQUE

The rotary motion is based on a USPM motor. However, the flux bridges in the rotor/mover designed for a linear motion will cause magnetic flux leakage II at the axial end. To study how the flux bridge affects the rotary motion, an RL-SVCM model without a flux bridge is proposed for comparison. The stator remains unchanged, and the rotor/mover has the same dimensions and PM. The rotor/movers are shown in figure 11.

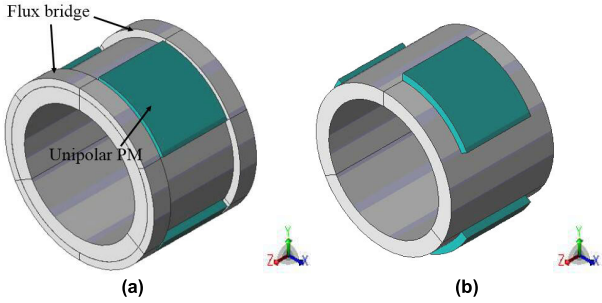

FIGURE 11. RL-SVCM rotor/mover structure: rotor (a) with and (b) without a bridge.

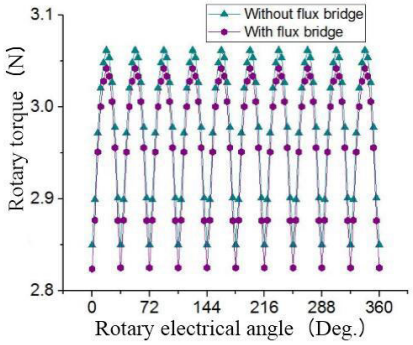

FIGURE 12. Torque comparison between with and without the flux bridge.

Figure 12 and Table 3 illustrate the rotary torque comparison between with and without a flux bridge, which is at the midpoint of the axial position. It was found that the torque curves basically coincide. The average torque of the model without a flux bridge is 2.980 N, and the torque ripple

TABLE 3. Electric machine parameters of RL-SVCM.

Item	Unit	With flux bridge	Without flux bridge
Rotary torque (axial midpoint)	N	2.958	2.980
Rotary torque ripple (axial midpoint)		7.3%	7.1%

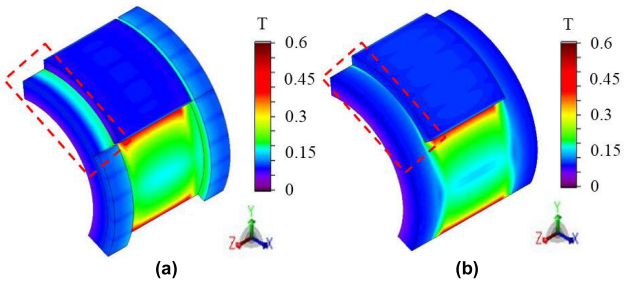

FIGURE 13. Rotor flux density distributions: rotor with and (b) without a flux bridge.

is 7.1%. The torque ripple is small. These are slightly higher than the model with a flux bridge at 2.958 N torque and a 7.3% torque ripple. The flux density distributions of these two rotors are shown in figure 13, where some PM leakage flux across the bridges occurs in the with-flux bridge model. For this reason, the torque increases slightly in the model without a flux bridge, but the effect is extremely small (0.7% bigger than the torque in the model with a flux bridge).

Figure 14(a) shows the back-EMF of the rotary motion. Figure 14(b) shows a comparison of the models with and without a flux bridge. It can be seen that the cogging torque is approximately 0.04 N peak to peak, and the flux bridges do not affect the cogging torque.

D. FEM ANALYSIS OF ROTARY AND LINEAR MOTIONS

1) FEM ANALYSIS OF ROTARY TORQUE

To analyze the interactions between the linear and rotary motions, different load currents and positions of the RL-SVCN were simulated. Table 4 shows the loss [30], [31] and efficiency of the RL-SVCM. Figure 15(a) shows the rotary torque distribution under a different rotary electrical angle versus different linear motion distances, as the motor operates under both linear and rotary motions. The rotary current circle is supplied by a five-phase sinusoidal current, and the linear voice coil current circle is supplied by a constant direct current. From figure 15(a), the rotary torque distribution on the axial linear distance has an extremely small fluctuation. The average torque is always approximately 2.94 nm, and the torque ripple is always 7.3% at different locations along the linear path. The motor always operates with a low torque ripple. This proves that any position of the RL-SVCM mover in the axial direction has almost no effect on the rotary output torque.

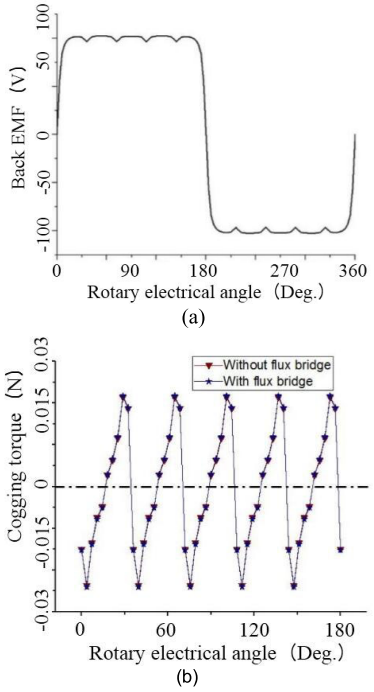

FIGURE 14. FEM result with no load (a) Back-EMF; (b) Cogging torque.

TABLE 4. Electric machine parameters of RL-SVCM.

Item	Unit	Value
Iron loss	w	12.12
Rotary coil copper loss	w	115.2
Linear coil copper loss (4A)	w	118.8
Rotary efficiency	%	81.6
Gross efficiency (4A)	%	69.8

Figure 15(b) shows the rotary torque distribution under different rotary electrical angles versus different linear voice coil currents at the midpoint of the axial position. The rotary current circle is also supplied by a five-phase sinusoidal current, and the linear voice coil circle is supplied by a gradually increasing current (at intervals of 0–8 A). It can be seen in figure 15(b) that the rotary torque does not have any effect on the change in the linear voice coil current. This shows that the voice coil current has no effect on the rotational motion.

From the figure 15(a) the torque ripple is always 7.3% under the rotary electoral angle. The ripple of rotary torque distribution on the axial linear distance is 1%. As well as, from the figure 15(b) the ripple of rotary torque under different voice coil current is 0.6%. Compared with [4]–[11], the proposed model has lower torque ripple.

2) FEM ANALYSIS OF LINEAR FORCE

Figure 16(a) shows the linear force distribution under different linear motion distances versus different rotary electrical angles, in which the linear voice coil circle is supplied by a constant current of 8 A. From this figure, the linear force reaches the minimum value at the axial midpoint when the

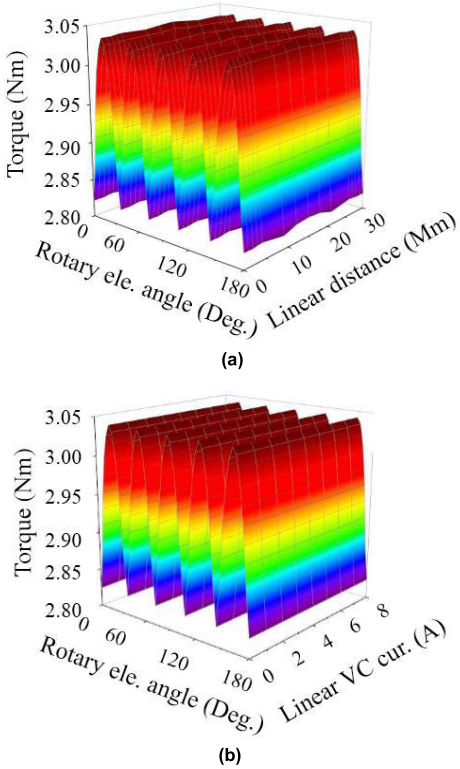

FIGURE 15. Rotary torque distribution: under different linear distance and (b) current.

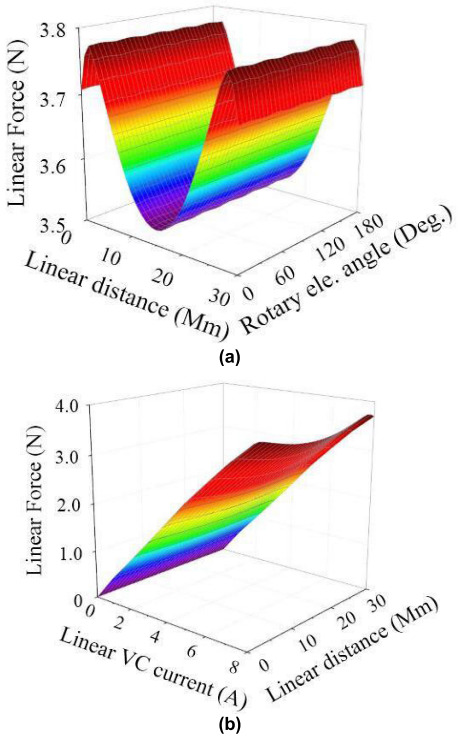

FIGURE 16. Linear force distribution; (a) under different rotary electrical angle; (b) under different linear current.

motor works at any rotary electrical angle. Despite changes in the rotary electrical angle, the linear force waveform will

always be the same. Therefore, a linear motion with a constant current does not have any effect on the rotary electrical angle distribution.

Figure 16(b) shows the linear force distribution under different constant currents versus different axial linear distances. From this figure, it can be observed that the linear force reaches the minimum value at the middle point of the axial position under any constant current. In addition, the force almost linearly changes as the current increases. It can be seen that the change in the force in the axial position is not affected by the magnitude of the voice coil current.

From figure 16(a), the force ripple is always 6.9% under linear distance. The ripple of linear force distribution on the rotary electoral angle is 0.03%. Compared with [4]–[11], the proposed model has smooth linear force.

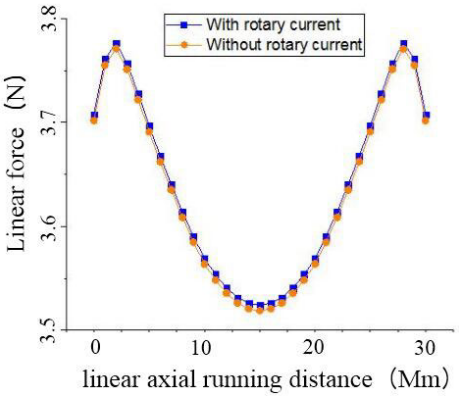

FIGURE 17. Linear motion forces comparison of with and without rotary current.

Figure 17 shows the linear force comparison of models with and without rotary five-phase current. The two curves in the figure basically coincide, and the average torque has a difference of only 0.1%. This is sufficient to show that the rotating five-phase current does not affect the linear force.

V. CONCLUSION

This article proposed a rotary-linear motor based in a single air-gap structure for achieving a simple structure, a low torque ripple, and a smooth linear force. The RL-SVCM combines a unipolar SPM motor and a voice coil motor structure. The MEC method was used to analyze the linear force distribution and effect of the flux bridges on the linear force and rotary torque. The FEM method is used to analyze the precise output result of rotary torque and linear force, which all keep in small ripple. The FEM results of the motor under rotary and linear motions were analyzed. It was found that the linear and rotary movements do not affect each other.

REFERENCES

[1] Y. Zheng and J. Duan, "Materials and fabrication issues of micro V-groove for optoelectronics packaging," *Adv. Mater. Res.*, vols. 295–297, pp. 1330–1334, Jul. 2011.

[2] J. Lee and S. Wang, "Topological shape optimization of permanent magnet in voice coil motor using level set method," *IEEE Trans. Magn.*, vol. 48, no. 2, pp. 931–934, Feb. 2012.

[3] L. Xie, J. Si, Y. Hu, and Z. Wang, "Overview of 2-degree-of-freedom rotary-linear motors focusing on coupling effect," *IEEE Trans. Magn.*, vol. 55, no. 4, pp. 1–11, Apr. 2019.

[4] S. Tanaka, T. Shimono, and Y. Fujimoto, "Development of a cross-coupled 2DOF direct drive motor," in *Proc. IECON-40th Annu. Conf. IEEE Ind. Electron. Soc.*, Dallas, TX, USA, Oct. 2014, pp. 508–513.

[5] M. Mori, W. Kitagawa, and T. Takeshita, "Characteristic analysis of 2-degree-of-freedom cylindrical actuator," in *Proc. 16th Int. Symp. Appl. Electromagn. Mech.*, 2014, vol. 45, nos. 1–4, pp. 257–264.

[6] J. Si, L. Xie, X. Xu, Y. Zhu, and W. Cao, "Static coupling effect of a two-degree-of-freedom direct drive induction motor," *IET Electr. Power Appl.*, vol. 11, no. 4, pp. 532–539, Apr. 2017.

[7] J. Si, L. Xie, J. Han, H. Feng, W. Cao, and Y. Hu, "Mathematical model of two-degree-of-freedom direct drive induction motor considering coupling effect," *J. Electr. Eng. Technol.*, vol. 12, no. 3, pp. 1227–1234, May 2017.

[8] L. Xu, M. Lin, X. Fu, and N. Li, "Design and analysis of a double-stator linear–rotary permanent-magnet motor," *IEEE Trans. Appl. Supercond.*, vol. 26, no. 4, pp. 1–4, Jun. 2016.

[9] L. Xu, M. Lin, X. Fu, and N. Li, "Analysis of a double stator linear rotary permanent magnet motor with orthogonally arrayed permanent magnets," *IEEE Trans. Magn.*, vol. 52, no. 7, pp. 1–4, Jul. 2016.

[10] L. Xu, M. Lin, X. Fu, K. Liu, and B. Guo, "Analysis of the end-effects in double stator linear-rotary permanent magnet motor with long mover," in *Proc. IEEE Conf. Electromagn. Field Comput. (CEFC)*, Miami, FL, USA, Nov. 2016, p. 1.

[11] M. M. Nezamabadi, E. Afjei, M. R. Naemi, and A. A. Afjei, "Design and 3D-FEM analysis of a rotary–linear switched reluctance motor," in *Proc. Int. Symp. Power Electron., Electr. Drives, Autom. Motion (SPEEDAM)*, Anacapri, Italy, Jun. 2016, pp. 430–434.

[12] M.-Z. Luo, H.-B. Zhou, J.-A. Duan, and B.-Q. Kou, "Design and analysis of a servo control system for a novel linear-rotary voice coil motor," in *Proc. 19th Int. Conf. Elect. Mach. Syst. (ICEMS)*, Chiba, Japan, Nov. 2016, pp. 1–5.

[13] Z.-J. Zhang, H.-B. Zhou, J.-A. Duan, and B.-Q. Kou, "Design and analysis of two-degree-of-freedom voice coil motors for linear-rotary motion," in *Proc. 19th Int. Conf. Elect. Mach. Syst. (ICEMS)*, Chiba, Japan, Nov. 2016, pp. 1–6.

[14] Y.-D. Chen, C.-C. Fuh, and P.-C. Tung, "Application of voice coil motors in active dynamic vibration absorbers," *IEEE Trans. Magn.*, vol. 41, no. 3, pp. 1149–1154, Mar. 2005.

[15] H.-C. Yu, T.-Y. Lee, S.-J. Wang, M.-L. Lai, J.-J. Ju, D.-R. Huang, and S.-K. Lin, "Design of a voice coil motor used in the focusing system of a digital video camera," *IEEE Trans. Magn.*, vol. 41, no. 10, pp. 3979–3981, Oct. 2005.

[16] R. Banik and D.-G. Gweon, "Design and optimization of voice coil motor for application in active vibration isolation," *Sens. Actuators A, Phys.*, vol. 137, no. 2, pp. 236–243, Jul. 2007.

[17] Q. Chen, G. Xu, G. Liu, W. Zhao, L. Liu, and Z. Lin, "Torque ripple reduction in five-phase IPM motors by lowering interactional MMF," *IEEE Trans. Ind. Electron.*, vol. 65, no. 11, pp. 8520–8531, Nov. 2018.

[18] Q. Chen, G. Liu, W. Zhao, and G. Xu, "Separation and comparison of average torque in five-phase IPM machines with distributed and fractional slot concentrated windings," *IET Electr. Power Appl.*, vol. 13, no. 3, pp. 285–293, Mar. 2019.

[19] G. Liu, L. Liu, Q. Chen, and W. Zhao, "Torque calculation of five-phase interior permanent magnet machine using improved analytical method," *IEEE Trans. Energy Convers.*, vol. 34, no. 2, pp. 1023–1032, Jun. 2019.

[20] Z. Zhang, C. Xia, H. Wang, and T. Shi, "Analytical field calculation and analysis of surface inset permanent magnet machines with high saliency ratio," *IEEE Trans. Magn.*, vol. 52, no. 12, pp. 1–12, Dec. 2016.

[21] M. Si, X. Yang, S. Zhao, and J. Si, "Development of the equivalent magnetic circuit model for a surface-interior permanent magnet synchronous motor," in *Proc. 6th Int. Conf. Power Electron. Syst. Appl. (PESA)*, Dec. 2015, pp. 1–4.

[22] J.-W. Jung, H.-I. Park, J.-P. Hong, and B.-H. Lee, "A novel approach for 2-D electromagnetic field analysis of surface mounted permanent magnet synchronous motor taking into account axial end leakage flux," *IEEE Trans. Magn.*, vol. 53, no. 11, pp. 1–4, Nov. 2017.

[23] A. Hemeida and P. Sergeant, "Analytical modeling of surface PMSM using a combined solution of Maxwell–s equations and magnetic equivalent circuit," *IEEE Trans. Magn.*, vol. 50, no. 12, pp. 1–13, Dec. 2014.

[24] B. Philips, "Bowers B. Philips technical review," *Techn. Rev.*, vol. 35, no. 4, pp. 77–95, 1975.
[25] N. Bianchi and T. M. Jahns, "Design, analysis, and control of interior PM synchronous machines," in *Proc. IEEE Ind. Appl. Soc. Annu. Meeting*, 3rd ed., Seattle, WA, USA, Oct. 2004, pp. 31–47.
[26] T. A. Lipo, *Introduction to AC Machine Design*. Madison, WI, USA: Univ. Wisconsin Madison, Electrical Engineering, 2011, ch. 9, pp. 401–453, doi: 10.1002/9781119352181.
[27] X. Sun, Z. Shi, G. Lei, Y. Guo, and J. Zhu, "Analysis and design optimization of a permanent magnet synchronous motor for a campus patrol electric vehicle," *IEEE Trans. Veh. Technol.*, vol. 68, no. 11, pp. 10535–10544, Nov. 2019.
[28] X. Sun, Z. Shi, G. Lei, Y. Guo, and J. Zhu, "Multi-objective design optimization of an IPMSM based on multilevel strategy," *IEEE Trans. Ind. Electron.*, early access, Jan. 15, 2020, doi: 10.1109/TIE.2020.2965463.
[29] K. Diao, X. Sun, G. Lei, Y. Guo, and J. Zhu, "Multiobjective system level optimization method for switched reluctance motor drive systems using finite element model," *IEEE Trans. Ind. Electron.*, early access, Jan. 1, 2020, doi: 10.1109/TIE.2019.2962483.
[30] X. Sun, Y. Shen, S. Wang, G. Lei, Z. Yang, and S. Han, "Core losses analysis of a novel 16/10 segmented rotor switched reluctance BSG motor for HEVs using nonlinear lumped parameter equivalent circuit model," *IEEE/ASME Trans. Mechatronics*, vol. 23, no. 2, pp. 747–757, Apr. 2018.
[31] S. Zhu, Y. Hu, C. Liu, and K. Wang, "Iron loss and efficiency analysis of interior PM machines for electric vehicle applications," *IEEE Trans. Ind. Electron.*, vol. 65, no. 1, pp. 114–124, Jan. 2018.

FUZHEN XING (Student Member, IEEE) was born in Liaoning, China, in 1991. He received the B.S. degree in electrical engineering from the Shenyang University of Technology, in 2014. He is currently pursuing the Ph.D. degree with the Department of Electronic Engineering, Hanyang University, South Korea. His research interest includes motor design and analysis.

BYUNG-IL KWON (Member, IEEE) was born in 1956. He received the B.S. and M.S. degrees in electrical engineering from Hanyang University, Ansan, South Korea, in 1981 and 1983, respectively, and the Ph.D. degree in electrical engineering, machine analysis from The University of Tokyo, Tokyo, Japan, in 1989. From 1989 to 2000, he was a Visiting Researcher with the Faculty of Science and Engineering Laboratory, University of Waseda, Tokyo. In 1990, he was a Researcher with the Toshiba System Laboratory, Yokohama, Japan. In 1991, he was a Senior Researcher with the Institute of Machinery and Materials Magnetic Train Business, Daejeon, South Korea. From 2001 to 2008, he was a Visiting Professor with the University of Wisconsin–Madison, Madison, WI, USA. He is currently a Professor with Hanyang University. His research interest includes design and control of electric machines.